Indian Journal of Chemical Technology
Vol. 26, March, 2019 pp. 111-121

Effect of cooling rate, particle size and volume fraction on non-isothermal crystallization of polypropylene/silica nanocomposite

Upasna Sharma & S J A Rizvi*

Polymer & Composite Material Laboratory, Department of Petroleum Studies, Aligarh Muslim University, Aligarh 202 002, India

E-mail: javedrizvi1976@gmail.com

Received 21 January 2018; accepted 10 December 2018

Thermoplastic nanocomposites of maleic anhydride grafted polypropylene (MA-g-PP) and monodisperse silica-nanospheres of diameter 60, 100 and 250nm have been prepared by melt blending in a twin screw micro-compounder. The tensile specimens are molded and tested using digital image correlation technique. The crystallinity has been determined using differential scanning calorimetry (DSC) and wide angle X-ray diffraction. The scanning and transmission electron micrographs show proper dispersion of silica-nanospheres in the matrix. Taguchi method has been employed for the analysis of non-isothermal crystallization parameters. The crystallization parameters are calculated from DSC plots. It is found from S/N ratio analysis that the increase in nanoparticle size leads to higher crystallinity, onset and peak temperature whereas reverse effect is observed for increase in cooling rate. The effect of volume fraction is less pronounced. Further it is found that the dependence of mechanical properties on interface between matrix and reinforcement is more decisive than crystallinity of nanocomposite.

Keywords: Non-isothermal crystallization kinetics, Differential scanning calorimetry, Taguchi's design of experiment, Signal to Noise response, Monodisperse silica-nanospheres

Polypropylene is a semi-crystalline polymer whose engineering applications are critically dependent on the degree of crystallinity[1]. When cooled from a melt, either isothermally or non-isothermally, it forms crystalline regions[2]. Since most of the polymer processing such as extrusion, injection molding, blow molding etc., are operated under non-isothermal condition therefore it is more close to the industrial conditions of the polymer processingin comparison to isothermal crystallization.

Nanoparticles help to enhance the crystallization ratedue to their higher surface area that offsets the decrease in free energy[3]. The presence of nanoparticle leads to heterogeneous nucleation mainly because of fluctuations in density. Primary nucleation involves the greatest surface area while the area is somewhat reduced for secondary nucleation. The tertiary nucleation, which can be defined as nucleation at an edge, involves further reduced specific area. The nanoparticles are compounded with pure polymer matrix, because the composite structure will reach higher rigidities and heat distortion temperature[4]. The stiffness or Young's modulus are readily improved by adding nanoparticlesbecause rigid inorganic particles generally have a much higher stiffness than polymer matrices. Silica nanoparticles are often used to increase the toughness and tensile performance of polypropylene[5]. By compounding silicananoparticles into the polypropylene matrix, its properties can be improved. The compounding can be done using three methods namely solution blending, in-situ polymerization[6] and melt compounding.

The size and volume of the nanoparticle added to the polymer are the parameters that affect the morphology of the nanocomposite and thus will affect the crystallization kinetics[7,8]. In addition, for the non-isothermal crystallization process, cooling rate is one of the most influential parameter to affecting the kinetics of crystallization[9-11]. The crystallization temperature and the cooling rate both have a great influence on crystallite size and shape[12,13]. The formation of large size spherulites was favored by slower cooling rate however smaller spherulites sizes result in better impact strength, higher crystallinity and higher elongation to break[14-16]. Nanoparticles reduce the degree of super cooling by increasing the onset temperature of crystallization which leads to faster crystallization[17]. These particles provide numerous nucleation sites around which PP chains can easily crystallize. The number of nucleating sites also increases the amount ofcrystallinity in the resin and decreases theaverage size distribution. Higher

crystallinity makes a material strong, but it causes brittleness[18,19]. A completely crystalline polymer would be too brittle to be used in real life applications. The amorphous regions contribute toughness inpolymer, that is, the ability to store strain energy without undergoing breaking.

In present work, the Taguchi method[20] for design of experiment was employed first time for the study of process variables affecting the non-isothermal crystallization parameters. The experiments were performed in a differential scanning calorimeter[21,22]. The selected factors namely particle size, volume fraction and cooling rate along with their individual levels are summarized in Table 2. The Avrami and Tobin parameters were also calculated. The signal-to-noise (S/N) responses were obtained from Taguchi analysis. The characteristic trends resulted from S/N ratio are quite meaningful for the optimization of polymer processing parameters in the light of desired crystallization parameters.

Experimental Section

Materials

The silica nanospheres were obtained from M/s. XL Sci-Tech-USA, in sizes of 60, 100, 250 nm with the tolerance of ±1 nm and were used as reinforcing agents. Polypropylene, with anhydride and acid functionality, was obtained from M/s. Pluss Polymers, India (trade name of OPTIM® P-406).The MFI of matrix was measured to be 40 g/10 min under standard test conditions of 2.16 kg, 190°C. The specific gravity of MA-g-PP was measured to be 0.91 and crystalline melting point was found to be around 163°C, from calorimetric measurements.

Compounding and molding of nanocomposite

The matrix (MA-g-PP) and silica nanospheres (0.03 and 0.05 vol. fractions) were tumbler mixed and vacuum dried for 8 h at 70°C and 50 mmHg to remove moisture before melt compounding. The conical co-rotating twin screw micro-compounder (make: DSM Research, Netherlands, model: 5 mL) was used for the melt compounding of various compositions of MA-g-PP/silica-nanospheres at the screw rpm of 130 and barrel temperature of 190°C for 10 min. The type-V, tensile test specimens were molded by microinjection molding system (Make: Thermo Electron Corp., Germany, Model: HAAKE MiniJet) at the barrel temperature of 200°C and the maximum injection pressure of 700 bar. Table 1 summarizes various injection molding parameters.

Characterization of MA-g-PP/silica-nanospheres nanocomposites

Morphological characterization

The transmission electron microscopy (TEM) and scanning electron microscope (SEM) were used for the morphological characterization of nanocomposite specimens. The samples for TEM were microtomed using ultra microtome (Make: Leica EM UC6, Germany) and were fixed onto a copper grid of 3.0 mm. The samples were scanned on TEM (Make: JEM-2100, JEOL) operated at an acceleration voltage of 200 kV. SEM analysis was carried out using SEM LEO 1430 VP instrument. Figures 1 and 2 show the

Table 1 — Injection molding parameters.

Molding parameters	Set point values
Melt temperature	200°C
Max. Injection pressure	700 bar
Packing pressure	350 bar
Cooling time	12 s

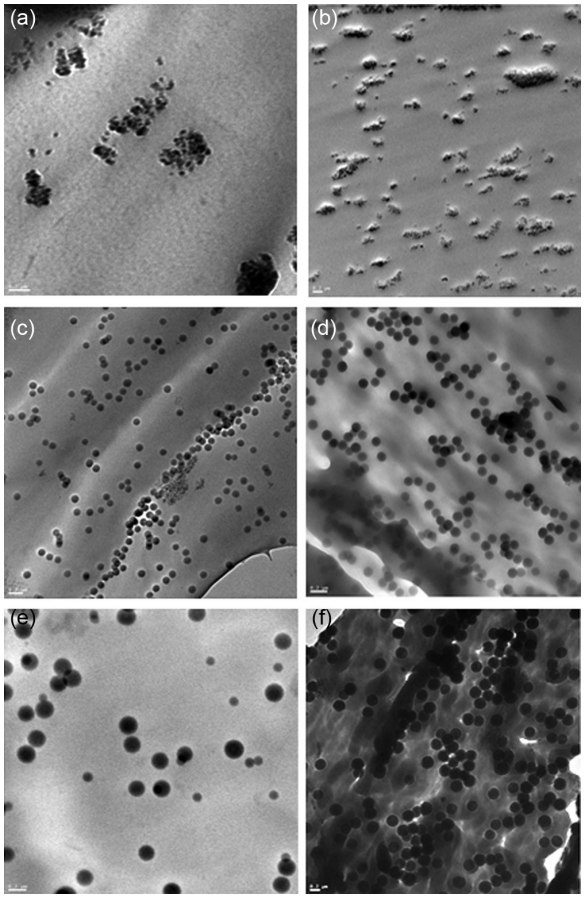

Fig. 1 —TEM microphotograph of MA-g-PP/silica-nanospheres (a). 60 nm, 3 vol. % (b). 60 nm, 5 vol. %, (c). 100 nm, 3 vol. % (d). 100 nm, 5 vol. %., (e). 250 nm, 3 vol. % (f). 250 nm, 5 vol. %.

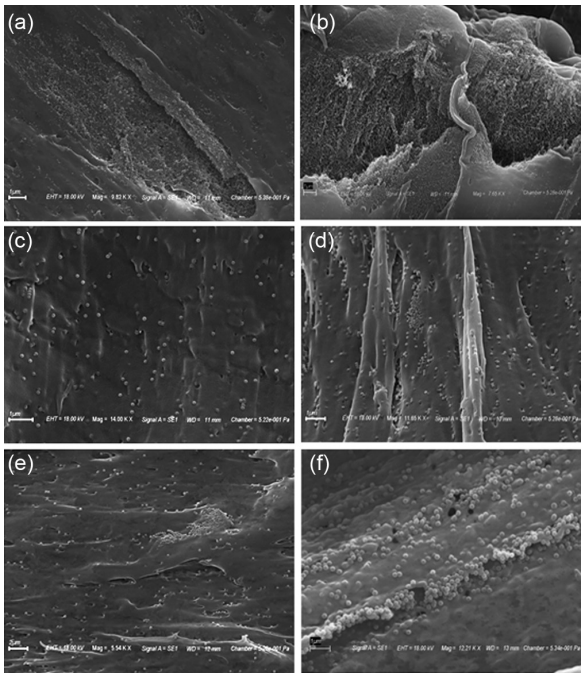

Fig. 2 — SEM microphotograph of MA-g-PP/silica-nanospheres (a). 60nm, 3 vol. % (b). 60nm, 5 vol. %, (c). 100nm, 3 vol. % (d). 100 nm, 5 vol. %., (e). 250 nm, 3 vol. % (f). 250 nm, 5 vol. %.

TEM and SEM micrographs of 60, 100 and 250 nm silica nanospherical particles with volumetric loading of 3 and 5%.

Wide angle X-ray scattering (WAXD)

The WAXD of MA-g-PP/ silica-nanospheres nanocomposites was performed to obtain the relative crystallinity. The X-ray diffraction was carried out for scan range (2θ) = 5° to 60° with the scan speed 1.0 degree.min-1. A Rigaku MINIFLEX-II powder diffractometer having an X-ray tube producing monochromatic Cu-Kα (λ = 1.54 A°) radiation was used for the study of nanocomposite. The neat MA-g-PP and nanocomposites samples were mounted onto sample stage to record the diffraction patterns and crystallinity index. It can be easily seen from the Fig. 3 that neat MA-g-PP has highest crystallinity whereas nanocomposite of MA-g-PP/ 60nm silica-nanospheres with 5 wt. % was found to be least crystalline.

Testing for mechanical properties

Neat MA-g-PP and its nanocomposites were tested for tensile properties. In order to minimize the errors during the measurement of strain, the DIC technique (digital image correlation) was used for contactless displacement readings. The samples were first painted with white color background by a normal spray and then black dots were spray painted on them by the

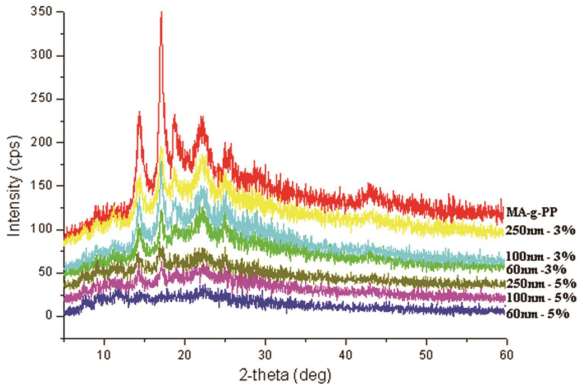

Fig. 3 — WAXD diffractograms of neat MA-g-PP and its nanocomposites.

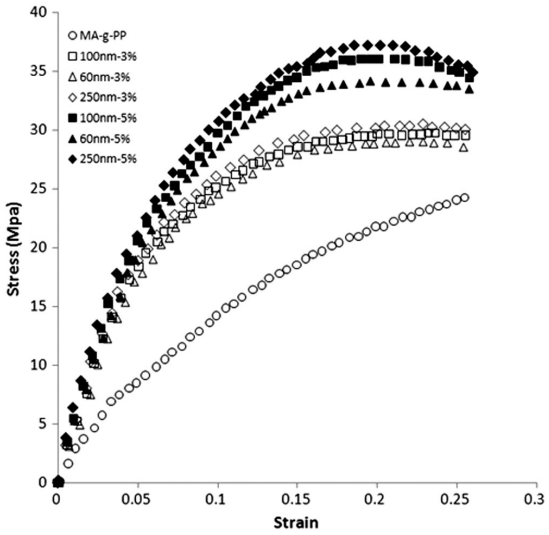

Fig. 4 — Stress-strain plot for neat MA-g-PP and its nanocomposites.

pneumatic painter gun. The samples were then dried and taken to the Universal Material Tester (make CETR, USA) for uniaxial tensile testing. The carriage was programmed to move up by a speed of 0.01 mm/s. A 5.0 mega pixel camera with strain measurement resolution of 25 microstrain was used to capture the displacement field during the test. The scale used was 2.8 micro meter per pixel. Later the displacement field was differentiated to obtain strains using the Lagrange strain tensor. Stress strain curve for 3 and 5 vol. % of nanocomposites are shown in Fig. 4.

Differential scanning calorimetric measurements

The DSC scan data files for MA-g-PP and its nanocomposites were obtained from Perkin-Elmer pyris 6000, differential scanning calorimeter (DSC). In order to unearth the effect of process variables (cooling rate, particle size and volume fraction) on various nonisothermal crystallization parameters, experiments were performed in accordance with the

Taguchi's design of experiments. Table 2 summarizes Taguchi's L9 DOE and Table 3 summarizes the values of crystallization parameters.

The crystallization peak temperature of MA-g-PP was found to be around 110°C, whereas its value is above 115°C for all other nanocomposite samples. Figure 5 shows the crystallization exotherm for neat MA-g-PP (Run-0) and its nanocomposites (Run 1 to 9) as per experimental plan given in Table 2. The samples were initially heated up to 200°C at the rate of 40°C/min to melt the sample and then held for 10 minutes in order to remove all previous thermal history. Later on the samples were cooled at various cooling rates as per experimental plan.

Results and discussion

Nonisothermal crystallization parameters

The DSC crystallization exotherm well describes the crystallization kinetics. The crystallization kinetics is attributed by various crystallization parameters. Several meaningful conclusions can be drawn on the basis of these parameters. Figure 6 shows the schematic of a typical crystallization exotherm and some of the important crystallization parameters. In present study we have examined the effect of process variables (cooling rate, particle size and vol. fraction) on various crystallization parameters. The crystallization peak temperature (T_p), one of the frequent used crystallization parameter, is the temperature at peak maxima. Higher value of peak temperature is indicative of crystallization at higher temperature and maximum rate of crystallization at a given cooling rate. The onset temperature (T_{onset}) indicates the measurable start of crystallization. It is the temperature at first detectable deviation from the baseline. The value of $T_{onset} - T_p$is usually an indication of rate at which polymer crystallizes. The

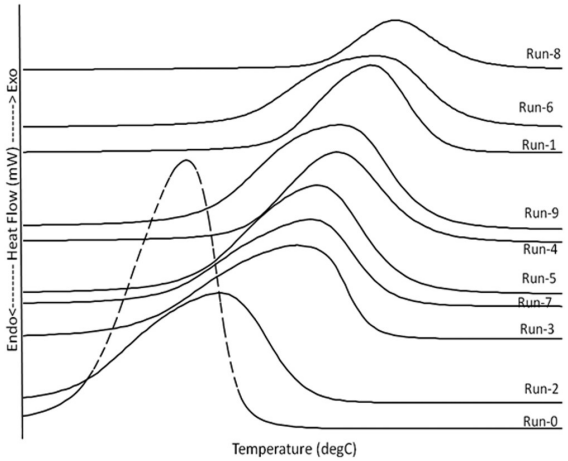

Fig. 5 — Stress-strain plot for neat MA-g-PP and its nanocomposites

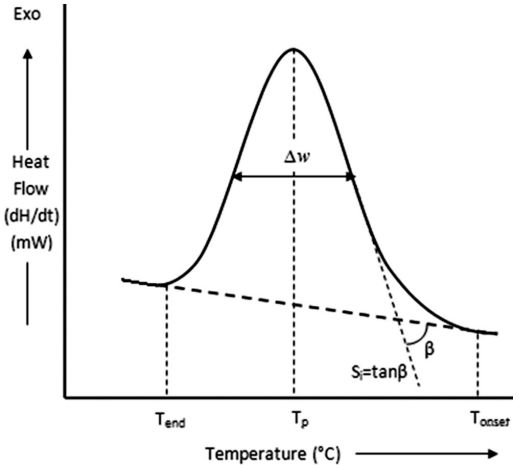

Fig. 6 — Schematic of nonisothermal crystallization exotherm.

Table 2 — Design of experiment: Taguchi's L-9 orthogonal array

Run	Particle size (nm)	% vol.	Cooling Rate (°C/min)
1	60	3	10
2	60	5	15
3	60	5	20
4	100	3	15
5	100	5	20
6	100	5	10
7	250	3	20
8	250	5	10
9	250	5	15

Table 3 — Summary of crystallization parameters obtain from DSC thermogram as per Taguchi's L-9 DOE.

Run	T_p (°C)	$T_{onset,}$ (°C)	T_{onset} -T_p	Δw	S_i	T_m	T_m -T_p	ΔH_m (J/g)	ΔH_c (J/g)	X_c (%)
0	110.51	117	6.49	6.09	3.732	177.73	67.22	63.31	-83.98	30.29
1	122.07	130	7.93	6.5	3.077	171.12	49.05	53.25	-66.82	26.26
2	112.7	123	10.3	9.26	2.904	179.21	66.51	43.03	-74.56	21.67
3	117.9	127	9.1	9.68	4.01	173.25	55.35	35.5	-48.16	17.87
4	120.1	131	10.9	6.76	2.144	171.27	51.17	58.86	-78.49	29.03
5	119	131	12	8.35	3.732	165.2	46.2	55.5	-72.75	27.95
6	123	134	11	9.17	2.144	169.07	46.07	46.81	-64.94	23.57
7	118.6	129	10.4	9.02	4.51	167.33	48.73	50	-40.81	24.66
8	124	133	9	5.5	0.932	164	40	77.6	-55.2	39.08
9	120.5	133	12.5	9.25	3.487	173.11	52.61	57.18	-76.73	28.80

Δw is the width at half height of the exotherm peak and a measure of crystallite size distribution. Smaller Δw indicates a narrow crystallite size distribution.S_i is the slope of initial linear section of the exotherm and is an indicative of nucleation rate.ΔH_c, is the amount of heat librated during crystallization process. It is also known as enthalpy of crystallization (J/g).

The degree of crystallinity (X_c) was calculated using following equation;

$$X_c = (\Delta H_m / \Delta H_m^o (1 - \emptyset)) \times 100 \quad \ldots (1)$$

where ΔH_m is the melting enthalpy of sample, $(1 - \emptyset)$ is weight fraction of polymer and ΔH_m^o is the theoretical melting enthalpy value for a 100% crystalline polymer, which is taken to be 209 J/g. Table 3 summarizes the values of various crystallization parameters for different experimental runs (1 to 9) according to Taguchi's design of experiments. Run 0 is for pure MA-g-PP matrix at cooling rate of 20°C/min.

S/N ratio analysis for nonisothermal crystallization parameters

The results of calorimetric experiments (Table 3) were analyzed for signal to noise (S/N) ratio. The outcomes of analysis are summarized in Fig. 7. The analysis indicates that the peak crystallization temperature increases with the size of silica-nanospheres and reduces with increase in vol. fraction of filler. Also the minimum S/N ratio for peak temperature is at cooling rate of 15°C/min. Thus it can be concluded that highest peak temperature is obtained in case of 3 vol. % and 250 nm silica-nanospheres, added to the polypropylene matrixandcrystallized at cooling rate of 10°C/min. Figure 7(b) shows the dependency of onset temperature (T_{onset}) on the particle size, volume fraction, and cooling rate. It has got similar behavior as in case of peak temperature except the fact that onset temperature does not change appreciably with volume fraction. It can be seen from Figs 1 and 2 that silica-nanospheres are uniformly distributed in 3 vol. % nanocomposites. Also the WAXD diffractograms shown in Fig. 3 clearly indicates that 5 vol. % nanocomposites are less crystalline. Therefore it can be concluded that possible agglomeration in case of 5 vol. % nanocomposites is actually responsible for equalizing the surface area of 3 and 5 vol. % nanocomposites available for nucleation. This leads to almost same value of S/N ratio for 3 and 5 vol. % nanocomposites.Another derived parameter is $T_{onset} - T_p$ and the reduced value indicates faster rate of crystallization. In most of polymer processing operations, a faster rate of crystallization is preferred therefore S/N ratio was carried out based on the

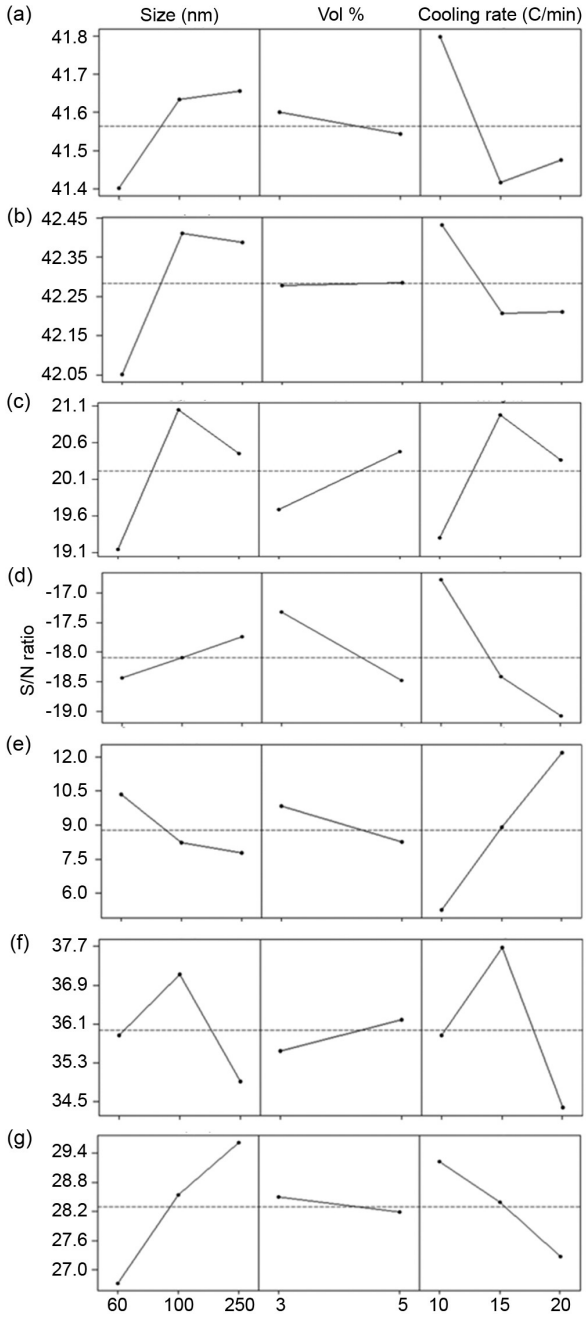

Fig. 7 — S/N ratio response for the effect of particle size, vol. % and cooling rate on (a) Peak temperature (*Tp*); (b) Onset temperature; (c) (*Tonset -Tp*); (d) Half width of crystallization (Δw); (e) Slope of exotherm (S_i); (f) Enthalpy of crystallization (ΔH_c) and (g) Percentage crystallinity (X_c).

algorithm of 'smaller is better'. Figure 7(c) shows that the 5 vol. % nanocomposite of 100nm size of silica-nanospheres yields highest rate of crystallization when cooled at the rate of 15°C/min. Figure 7(d) shows the S/N ratio variation for half widthof crystallization (Δw) with respect to the process variables.A smaller value of Δw indicates narrow and uniform distribution of crystallites. The physical properties of polymer nanocomposites are better when crystallite distribution is narrow therefore again the 'smaller is better' algorithm was used for S/N ratio analysis. The S/N ratio increases with the increase in particle size and decreases with increase in volume fraction of silica-nanospheres. Also indicates that a slower cooling rate leads to narrow and more uniform distribution of crystallites in nanocomposites. The slope of initial linear section (Si) of crystallization exotherm is a measure of the rate of nucleation. Figure 7(e) shows faster rate of nucleation with smaller nano particle size and vol. % whereas a faster cooling rate enhances the rate of nucleation. A higher nucleation rate leads to large number of smaller crystals. In packaging industry it is advantageous to have transparent packaging in most of the cases. Since transparency is directly related with ratio of wave length of light and crystal size. Therefore most of the nucleating agents produce the similar effect in polypropylene that leads to smaller crystals of high population density in typical range of cooling rate usually encountered in polymer processing industries. Figure 7(f) shows S/N ratio analysis for enthalpy of crystallization. It is actual amount of heat per unit mass liberated during the crystallization as a result of reduction in entropy leading to stable crystal structure. Higher value of ΔHc indicates more crystalline structure. It can be seen that most favorable condition for crystallization of MA-g-PP/ silica-nanospheres nanocomposite is 100nm size of silica-nanospheres with 5 vol. % loading in matrix and cooling rate of 15 °C/min within the limitations of present study. Figure 7(g) shows the analysis result for percentage crystallinity calculated on the basis of melting enthalpy given in Eq. (1). The melting enthalpy of 100% crystalline polypropylene was taken as 207 J/g. According to this analysis it can be concluded that increase in particle size favors percentage crystallinity whereas increase in cooling rate affects the percentage crystallinity adversely. A slight decrease in percentage crystallinity with volume fraction is also seen.

S/N ratio analysis for Avrami parameters

The most frequent quantitative evaluation of crystallization is done by applying the Avrami equation to isothermal crystallization. Since most of the polymer melt-processing methods work non-isothermally therefore attempts have been made by researchers to extend the Avrami model for nonisothermal crystallization. Since both the nucleation and crystal growth are affected by change in temperature, it leads to significant curvature in Avrami plots. According to this model, Eq. (2) is used to determine the crystallization kinetics, where the parameter Z_t is the crystallization or growth rate constant and is a temperature dependent term whereas n represents the Avrami exponent that contains information on nucleation type and growth geometry, but not on the amount of nucleation. For nonisothermal crystallization, Avrami equation does not account for the secondary crystallization, but it is valid only for early stages of crystallization.

$$X(t) = 1 - \exp(-Z_t t^n) \quad \ldots (2)$$

Eq. (2) can be modified to fit the equation of straight line, as shown in Eq. (3);

$$\log[-\ln(1 - X_t)] = n\log Z_t + n\log t \quad \ldots (3)$$

The plot of log [$-ln\ (1-X_t)$] vs. log t, at various cooling rates, we obtain the straight line. The slope and intercept values of straight line are the Z_t and n values in Avrami model. Since nonisothermal crystallization involves transient temperature but Avrami rate constant (Z_t) is independent of cooling rate. Therefore a corrected Avrami rate constant Z_c has been proposed that accounts for change in temperature during crystallization.

$$\log Z_c = \log Z_t / \alpha \quad \ldots (4)$$

where α is the cooling rate. The crystallization half time$t_{1/2}$ can be defined as the time to reach half of the crystallization and can be calculated using Z_c, and the relation is shown in Eq. (5);

$$t_{1/2} = (ln2/Z_c)^{1/n} \quad \ldots (5)$$

In order to quantitatively evaluate effect of process variable on Avrami parameters, Eq. (3) was used to

plot straight lines for different experimental runs as per Taguchi's design of experiment registered Table 2. And the values of Avrami parameters were determined using Eq. (4 & 5). Table 4 contains the values for nonisothermal crystallization parameters for neat MA-g-PP (run-0) and it's various nanocomposites (run 1-9). The Avrami plots are shown in Fig. 8.

At the early stage of crystallization, log [$-ln\ (1-X_t)$] is in a good linear relation with log(t), indicating that the modified Avrami equation is suitable for these composites. The physical meanings of Z_t and n cannot be related to the non-isothermal case in a simpleway as in case of isothermal crystallization, although their use provides further insight into the kinetics ofnon-isothermal crystallization. At the start of crystallization process there is a free energy threshold that needs to be overcome for nuclei to start growing. Density fluctuation across the melt help to overcome this barrier and leads to formation of primary nuclei, and the process is known as primary nucleation. Secondary nucleation refers to growth of a new layer of a polymer crystal on primary nuclei while tertiary nucleation involves attachment of polymer segments to the edges of a growing crystal. The nucleation in the presence of foreign particles is termed as heterogeneous nucleation. All the polymer composites (micro or nano) belong to this category whereas neat polymers undergo homogenous nucleation. The time dependency of nucleation refers to either 'thermal' or 'athermal' type of nucleation. Thermal nucleation refers to nucleation process that continues throughout the crystallization process while athermal nucleation refers to initiation and growth of all the crystals at same time. Homogenous nucleation is always thermal and heterogeneous nucleation is athermal in most of the cases.

The higher value of Avrami's growth rate constant 'Z_c' leads to faster crystallization, therefore for S/N ratio response 'larger the better' algorithm was selected for Z_c and n. Whereas, for half time of crystallization time '$t_{1/2}$', 'smaller the better' algorithm was selected. Figure 9 shows the S/N ratio response for particle size, vol. % and cooling rate on Avrami's parameters.

According to Fig. 9(a) the Avrami exponent (n) increases with the increase in size of silica-nanospheres and cooling rate whereas it remains indifferent with volume fraction of nano particles. The value of Avrami exponent varies from 2.277 to 4.239. It indicates that the type of nucleation changes from two dimensional lamellar structure to three dimensional spherulitic crystal structure. Figure 9(b) shows that corrected Avrami growth rate constantZ_c decreases with the increase in volume fraction of silica-nanospheres. This finding is in good agreement with the outcome of S/N response for S_i shown in Fig. 7(e). Further the S/N response for Z_c is found to be maximum for 100 nm size of silica-nanosphere.

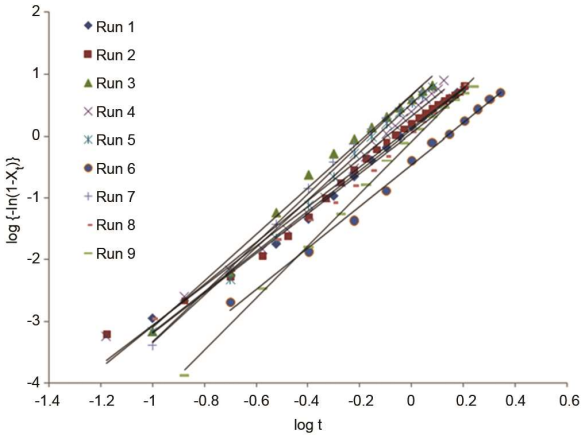

Fig. 8 — Avrami plots of log [$-ln\ (1-X_t)$] against log t forMA-g-PP/ silica-nanosphere nanocomposite.

Table 4 — Results for Avrami analysis of nonisothermal crystallization kinetics

Run	Size(nm)	% vol.	Cooling rate (°C/min)	Avrami Parameters		
				n	Z_c	$t_{1/2}$ (s)
0	MA-g-PP	-	20	3.791	1.04210	53.88
1	60	3	10	2.277	1.0076	53.52
2	60	5	15	3.931	0.99728	52.99
3	60	5	20	3.768	1.02053	54.14
4	100	3	15	3.395	1.01448	53.63
5	100	5	20	3.859	1.01548	54.34
6	100	5	10	3.384	1.03187	53.34
7	250	3	20	3.993	1.01939	54.47
8	250	5	10	3.240	1.00399	53.51
9	250	5	15	4.239	0.99711	55.06

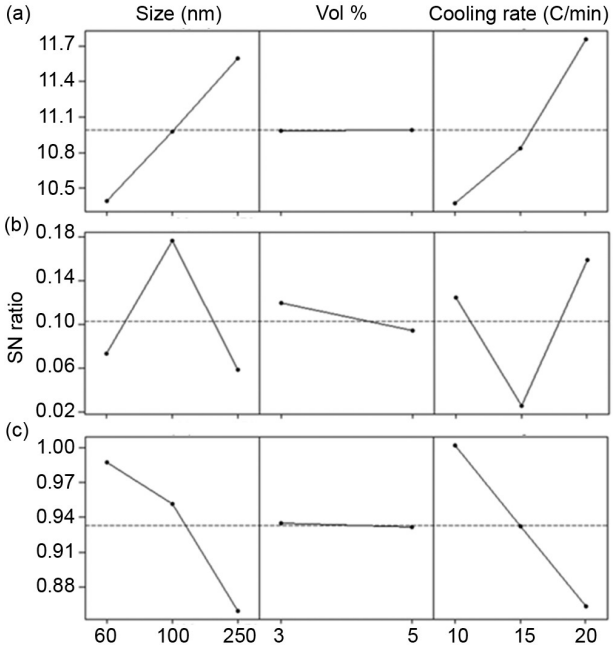

Fig. 9 — S/N ratio response showing the effect of particle size, vol. % and cooling rate on (a) Avrami exponent, *n*; (b) Avrami rate constant Z_c and (c) Half time of crystallization $t_{1/2}$.

The indication is in accordance to conclusion drawn for another parameter (T_{onset} - T_p) describing crystallization rate as shown in Fig. 7 (c). Half time of crystallization ($t_{1/2}$) is nearly indifferent with volume fraction of nanoparticle and found to be decreasing with increase in cooling rate and particle size.

4.4 S/N ratio analysis for Tobin parameters.

Another method was proposed by Tobin, for the analysis of nonisothermal crystallization kinetics with growth site impingement. It improves Avrami method which is valid only for early stages of crystallization. The expression proposed by Tobin is shown in Eq. (6);

$$X_t = (K_t t)^{n_t}/1 + (K_t t)^{n_t} \quad \ldots (6)$$

where 'K_t' and 'n_t' denotes the Tobin rate constant and exponent respectively. This equation can be converted to the equation of straight line, as expressed in Eq. (7);

$$\log[X_t/(1 - X_t)] = n_t \log t + n_t \log K_t \quad \ldots (7)$$

Tobin exponent and rate constant were evaluated by fitting the data in Eq. (7). The slope and intercept were calculated and used to find Tobin parameters. Various nucleation and growth mechanism governs the Tobin exponent; also it is not necessarily an integer. The Tobin plots are shown in Fig. 10 and analysis results are summarized in Table 5. The values of Tobin exponent ranged from 3.519 to 5.321 and rate constant ranged from 1.1672 to 1.9620. But here these parameters were not sufficient to describe the crystallization kinetics properly; therefore, these values were used to find the S/N ratio response that revealed the effect of size, volume % and cooling rate on Tobin parameters.

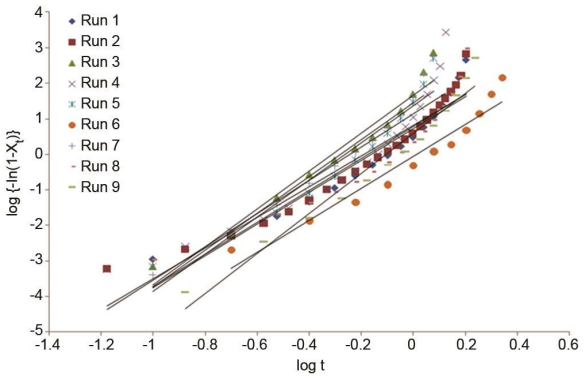

Fig. 10 — Tobin plots of log $[X_t/(1-X_t)]$ against log *t*forMA-g-PP/ silica-nanosphere nanocomposite.

Table 5 — Results for Tobin analysis of nonisothermal crystallization kinetics

Experiment _run	Size (nm)	% wt.	Cooling rate (°C/min)	Tobin parameters n_t	K_t
0	MA-g-PP	-	20	4.41	2.73931
1	60	3	10	4.498	1.48848
2	60	5	15	3.519	2.26725
3	60	5	20	5.321	2.04659
4	100	3	15	4.684	1.74880
5	100	5	20	5.210	1.82002
6	100	5	10	4.870	1.16720
7	250	3	20	5.165	1.89344
8	250	5	10	4.483	1.44672
9	250	5	15	4.951	1.14492

Greater values of rate constant suggests faster crystallization rate, hence larger the better algorithm was looked for S/N ratio response. Figure 11 shows the effect of Tobin exponent and Tobin growth rate constant.

Figure 11(a) shows that Tobin exponent was maximum when 3 vol. % of 100 nm size nano-silica particles were added to the MA-g-PP, and was processed at cooling rate 20°C/min, whereas Tobin exponent was minimum when the size of silica-nanosphere was 60 nm and its 5 vol. % was added to matrix and cooled at the rate of 15°C/min. However, Fig. 11(b) shows that on increasing the cooling rate and decreasing the percentage of amount of nano-particle in nanocomposite lead to faster rate of crystallization.

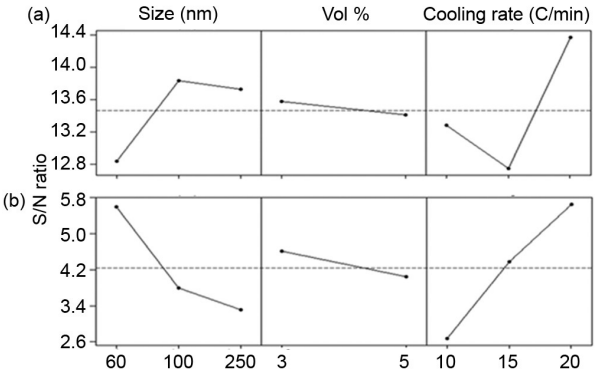

Fig. 11 — S/N ratio response showing the effect of particle size, volume% and cooling rate on (a) Tobin exponent, n_t and (b)Tobin rate constant, K_t

Tensile properties of MA-g-PP/ silica-nanosphere nanocomposites

To examine the any prevailing relationship between the crystallinity and physical properties ofMA-g-PP/ silica-nanosphere, tensile testing was carried. The WAXD diffractograms were referred side by side. The addition of silica-nanospheres in MA-g-PP matrix works as nucleating agents and leads to smaller size spherulities. These spherulities affect many mechanical properties of the material such as crystallinity, tensile strength and Young's modulus. Generally, these mechanical properties are found to increase with the addition of nanoparticles. This increase is due to the lamellae fraction within the spherulities, where the molecules are more densely packed than in the amorphous phase. Stronger intermolecular interaction within the lamellae accounts for increased hardness, but also for higher brittleness. On the other hand, the amorphous regions between the lamellae within the spherulities provide toughness to the material. Toughness is the property of material which provides it the ability to deform rather than break when it is subjected to stress.

Results obtained from tensile experiments for MA-g-PP and MA-g-PP/ silica-nanospheres nanocomposites are shown in Fig. 12. As can be seen, the introduction of silica-nanospheres increased the tensile modulus up to 17% for 3 vol. % and 33% for 5 vol. % nanocomposites. The improvement in tensile modulus is contributed by the inherent stiffness of silica nanoparticles and quality of dispersion mainly at low loading of nanoparticles. It was also observed that maximum and minimum value of tensile modulus was achieved when 5 vol. % of 60nm and 3 vol. % of 250 nm silica-nanospheres were added. Further it was

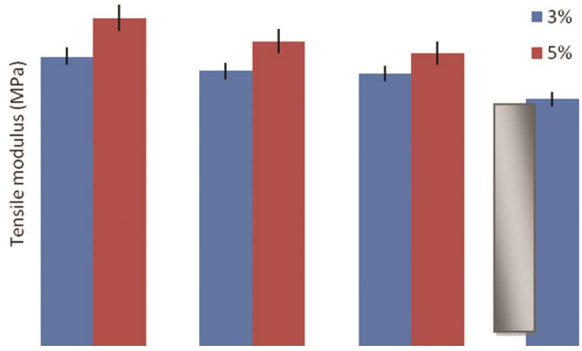

Fig. 12 — Tensile modulus of MA-g-PP and MA-g-PP/ silica-nanospheres nanocomposites.

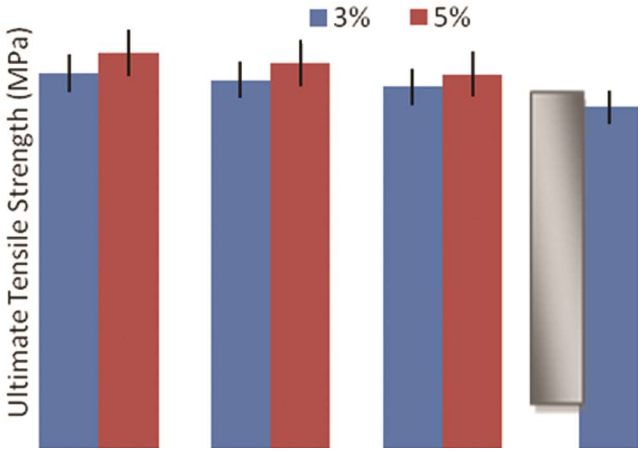

Fig. 13 — Ultimate tensile strength of MA-g-PP and MA-g-PP/ silica-nanospheres nanocomposites

noticed that tensile modulus increases with volume fraction of nanoparticle and decreases with the increase in particle size. This observation seems contradictory with the findings of X-ray scattering shown in Fig. 3. According the X-ray diffractograms nanocomposites of 5 vol. % are less crystalline as compared with 3 vol. %and crystallinity decreases with decrease in particle size. Since the tensile modulus represents stiffness which is directly related to the filler loading percentage and not highly influenced by the crystallinity therefore nanocomposites containing 5 vol. % of reinforcement exhibits higher value of modulus.

The ultimate strength strongly depends on the stress transfer between the nanoparticles and the matrix. The role of maleic anhydride is to increase the interfacial adhesion between the polypropylene matrix and silica-nanospheres. As it can be seen from the SEM and TEM images, in Fig. 2, nanoparticles are uniformly distributed without agglomeration especially at low percentage of reinforcement loading. Figure 13 shows the strength values of pure matrix

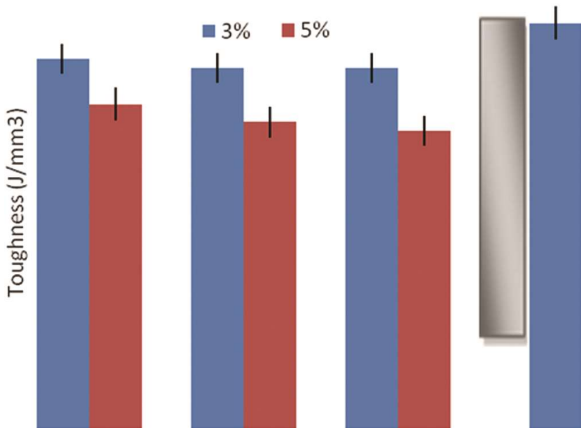

Fig. 14 — Toughness of MA-g-PP and MA-g-PP/ silica-nanospheres nanocomposites.

and nanocomposites were obtaned. It was observed that improvement in strength is only from 6% to 16%. Although the trend observed for strength is similar to the trend for tensile modulus. Again when the observed trend was analyzed in the light of X-ray diffractograms, it can be concluded that the strength of interface (interfacial shear strength), the quality of compatibilization and dispersion are more influential than the crystallinity of nanocomposites in determining the mechanical properties.

Another desirable property of material in real life applications is toughness. The key to toughness is a good combination of strength and ductility. A material with high strength and high ductility will have more toughness than a material with low strength and high ductility. It can be seen from Fig. 14 that toughness decreases with incorporation of silica-nanospheres in PP matrix. The addition of silica nanoparticles increases the stiffness of material at the cost of its ductility. In order to absorb the strain energy, the ability of material to undergo the deformation without break is must. Incorporation of nanosilica particles creates resistance to deformation because of their inherent stiff nature.

Conclusion

The thermal and mechanical properties as well as the morphology of MA-g-PP reinforced with different amount and sizes of silica-nanospheres have been studied. The results obtained from Taguchi experimental design yield crystal clear trends of crystallization parameters with the variation in three process variables namely the particle size, volume fraction and cooling rate. These three variables are easy to control at the time of industrial production of polymer nanocomposites. The results obtained in this study are very lucrative from industrial manufacturing point of view as the S/N responses quantitatively represent meaningful information about the nonisothermal crystallization parameters. The practicing polymer engineer or technologist can vary the aforesaid process variables to achieve the optimized crystallization parameters. Among the three process variables, the cooling rate and particle size are found to be most influential whereas some crystallization parameters (such as onset temperature, Avrami exponent and half crystallization time) were unaffected by volume fraction of nanoparticles while others have less pronounced effect of nanoparticle loading. It is also concluded that the tensile properties of MA-g-PP/ silica-nanosphere nanocomposites are mainly dependent on the properties of interface between the reinforcement and matrix than the crystallinity of material. Further it can be a useful hint for the polymer processors that they can take an informed decision to optimize the cooling rate for faster molding cycles at the cost of crystallinity. However an excellent set of interfacial properties achieved by proper compatibilization of reinforcement with matrix and uniform dispersion of nanoparticles without formation of agglomerates, are the prerequisites for good mechanical properties of nanocomposites.

References

1 Qiu S, Zheng Y, Zeng A & Guo Y, *Thermochimica Acta*, 512 (2011) 28.
2 Mubarak Y, Harkin-Jones E M A, Martin P & Ahmad M, *Polymer*, 42 (2001) 3171.
3 Antoniadis G, Paraskevopoulos K M, Bikiaris D & Chrissafis K, *Thermochimica Acta*, 510 (2010) 103.
4 Reynaud E, Jouen T, Gauthier C, Vigier G & Varlet J, *Polymer*, 42 (2001) 8759.
5 Papageorgiou G Z, Achilias D S, Bikiaris D N & Karayannidis G P, *Thermochimica Acta*, 427 (2005) 117.
6 Jain S, Goossens H, Duin M V & Lemstra P, *Polymer*, 46 (2005) 8805.
7 Weibing X, Mingliang G & Pingsheng H, *J Polym Sci., Part B: Polym Phys,* 40 (2002) 408.
8 Di Lorenzo M L & Silvestre C, *Progress in Polymer Science*, 24 (1999) 917.
9 Huang J W, Chang C C, Kang C C & Yeh M Y, *Thermochimica Acta*, 468 (2008) 66.
10 Drongelen M V, Erp T B V & Peters G W M, *Polymer*, 53 (2012) 4758.
11 Coccorullo I, Pantani R & Titomanlio G, *Polymer*, 44 (2003) 307.
12 Lonkar S P, Therias S M, Caperaa N, Leroux F, Gardette J L & Singh R P, *Polymer*, 50 (2009) 1505.
13 Lonkar S P & Singh R P, *Thermochimica Acta*, 491(2009) 63.

14 Kaur J, Lee J H & Shofner M L, *Polymer*, 52 (2011) 4337.
15 Van-der-wal A, Mulder J J, Oderkerk J & Gaymans R J, *Polymer*, 39(1998) 6781.
16 Wright D G M, Dunk R, Bouvart D & Autran M, *Polymer*, 29(1988) 793.
17 Zhang M, Liu Y, Zhang X, Gao J, Huang F, Song Z, Wei G & Qiao J, *Polymer*, 43 (2002) 5133.
18 Parenteau T, Ausias G, Grohens Y & Pilvin P, *Polymer*, 53 (2012) 5873.
19 Galeski A, *Prog Polym Sci*, 28 (2003) 1643.
20 Krishnaiah K & Shahabudeen P, *Applied design of experiments and Taguchi methods*, (PHI learning Pvt. Ltd., New Delhi) 2012.
21 Menczel J D &Prime R B, *Thermal Analysis of Polymers Fundamentals and Applications*, (John Wiley & Sons Inc., New Jersey) 2009.
22 Ehrenstein G W, Riedel G & Trawiel P, *Thermal Analysis of Plastics Theory and Practice*, (Carl Hanser Verlag, Munich) 2004.